High-resolution surface plasmon resonance sensor based on linewidth-optimized nanohole array transmittance

Kevin A. Tetz, Lin Pang, and Yeshaiahu Fainman

Department of Electrical and Computer Engineering, University of California, San Diego, California 92093

Received December 15, 2005; revised February 8, 2006; accepted February 11, 2006; posted March 1, 2006 (Doc. ID 66681)

A high spectral resolution, 2D nanohole-array-based surface plasmon resonance sensor that operates at normal or near normal incidence—facilitating high spatial resolution imaging—is presented. The angular and spectral transmittance of the structure is modified from a Fano type to a pure Lorentzian line shape with a parallel and orthogonal polarizer–analyzer pair. This change leads to a linewidth narrowing that maximizes the sensor resolution, which we show to be of $O(10^{-5})$ refractive index units (RIU). We estimate the potential of this system of $O(10^{-6})$ RIU under optimal conditions. © 2006 Optical Society of America

OCIS codes: 130.6010, 230.3990, 240.6680, 260.3910.

A wide variety of surface plasmon resonance (SPR) sensors have been demonstrated. The most common configurations employ the Kretschmann geometry or a shallow grating coupler and monitor the resonance shift (reflection minima) as a function of angle, wavelength, or simply as differential intensity.[1] More recent approaches have included phase sensitive variations, demonstrated in both interferometric[2] as well as ellipsometric configurations.[3] One major drawback with the conventional coupling methods is the difficulty in incorporating the sensor elements in high NA aperture imaging systems to increase spatial resolution and the corresponding number of resolvable spots. Operating on a prism or with a first-or higher-order diffraction mode places severe constraints on the depth of focus in the imaging system needed for large arrays of assays. Massive parallelism, and hence high throughput, is of primary importance in many potential SPR sensor applications, but they are severely limited by most of the current design configurations.[4,5]

Recently, Ebbesen *et al.*[6] demonstrated enhanced transmission through subwavelength hole arrays, which is generally attributed to the resonant excitation of surface plasmon polariton (SPP) waves. Such structures may be exploited for sensor applications due to their potential for significantly decreasing the interrogation volumes while operating at normal or near-normal illumination. This leads to a high packing density, minimal analyte volumes, and a large number of parallel channels while facilitating high-resolution imaging and wide field of view, supporting a large space–bandwidth product (SBP). These advantages may make such devices preferable in a number of applications despite the fact that the ultimate spectral resolution is lower than the prism-based equivalent because of SPR broadening due to both radiative and material damping. Several authors have suggested and demonstrated the use of subwavelength hole arrays for sensing applications,[7,8] and there are numerous numerical and experimental studies on their spectral properties. In this Letter we demonstrate a SPR sensor based on a metal film, perforated by a nanohole array, and specifically show polarization properties that facilitate narrowing the transmission linewidth (and hence maximize resolution) while operating in a regime that facilitates high SBP imaging.

Samples for our experiments are fabricated by depositing gold films of ~200 nm on glass substrate followed by spin coating and patterning by holographic lithography to achieve large usable areas (~1 cm^2). Multiple exposures of a chemically amplified negative resist (SU-8) yield a 2D array of nanoholes, and the exposure time and postexposure baking step allow fine control of the hole diameter[9] (~200 nm). To facilitate large SBP imaging, we choose the period a of the array to be close to the wavelength λ of the excitation field ($a/\lambda \sim 1$) with the fabricated value of $a = 1.4\ \mu m$. The developed SU-8 is used as a mask for etching nanoholes into the gold film by using inductively coupled plasma (ICP)/reactive ion etching (RIE) dry etching, and a polydimethylsiloxane (PDMS) mold with a microfluidic delivery channel $1\ cm \times 2\ mm \times 100\ \mu m$ is then bonded to the substrate by an oxygen plasma. Measurements are carried out using a simple setup shown in Fig. 1, where a collimated, tunable laser source (1520–1570 nm, 6 dBm) of ~1 cm in diameter is used to excite a SPP field in the 2D nanohole array. The sample is inserted between a polarizer–analyzer pair, and the transmitted light is used to simultaneously image an area of $\sim 200\ \mu m \times 200\ \mu m$ of the sample onto an InGaAs camera for alignment as well as a photodiode for transmission measurements.[10] Angular interrogation is achieved using a mechanical rotation stage rotating the sample in the $y-z$ plane. We refer to two polarization states in our measurements. (i) Parallel polarizer–analyzer (PP): polarizer and analyzer axes are parallel and oriented at $+\pi/4$ with respect to the [1,0] direction of the nanohole array (see Fig. 1) yielding equal electric field amplitudes in the x and y directions. (ii) Orthogonal polarizer–analyzer (OP): the polarizer (analyzer) axis is oriented at $+\pi/4$ ($-\pi/4$) with respect to the [1,0] direction. Resonant transmittance through the 2D nanohole array depends on the interrogation angle and wavelength of

0146-9592/06/101528-3/$15.00

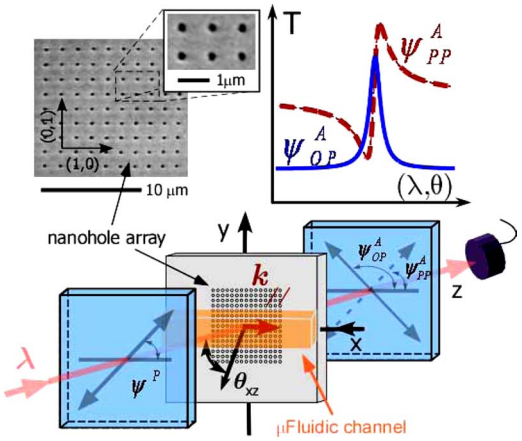

Fig. 1. (Color online) Conceptual diagram of the 2D nanohole-array-based SPR sensor. The input and output polarization states of a tunable laser are controlled, providing variable spectral or angular Fano-type profiles. A microfluidic channel is used to transport the analyte fluid to the surface of the sensing area and can be used to control the refractive index on the metal–dielectric interface to tune the SPP resonance frequency. Also shown is a scanning electron microscopy image of a representative sample.

radiation and has a Fano-type[11–13] line shape for PP and a Lorentzian shape for OP (see Fig. 1). There have been a number of studies that have investigated and explained the effects of the various geometric parameters on the shape of the resonant transmission (e.g., hole size, metal film thickness, and optical properties of the metal), and we note that the critical feature (assume a relatively "thick" film) is the hole diameter, which increases the scattering rate and hence broadens the resonance linewidth.[14] This resonant transmission mechanism, as elucidated by Barnes *et al.*,[15] involves coupling to an SPP mode, evanescent transmission through the below-cutoff waveguide hole, and scattering of radiation again from the hole array to produce propagating free-space modes. The surface wave is excited by a projection of the incident electric field polarization in the propagation direction,[16] and the reradiated field is again projected onto the analyzer. This effect has been explored previously with 1D gratings[17] and utilized in imaging SPPs excited on 2D SPP grating couplers.

Normalized transmittance spectra for both wavelength and angular interrogation are shown in Fig. 2 in the vicinity of $[-1,0]$ type SPP modes with an air overlayer. We observe a characteristic Fano shape for PP (dotted curves) and a pure Lorentzian shape for OP (solid curves); with OP the background contribution is suppressed, leaving only the resonance component of the transmission. The absolute transmittance is low, −23 dB (0.50%) for PP, due to the small size of the diameter of the holes (thus yielding relatively narrow lines), and drops to approximately −29 dB (0.13%) for OP due to additional polarization projection onto the analyzer. The extinction ratio of ~15–20 dB, limited by the linewidth as well as depolarization due to surface roughness in the etched holes, is shown in the inset of Fig. 2(b). Under wavelength interrogation the background level does not drop to the same deep minimum levels within the tuning range of our laser. The measured FWHMs for wavelength interrogation [Fig. 2(a)] are 1.28 meV (2.47 nm) and −2.86 meV (5.53 nm) for OP and PP, respectively, and the PP transmission peak is redshifted from that in OP by 0.40 meV (0.77 nm). Similarly, the measured FWHMs for angular interrogation [Fig. 2(b)] are 0.0012 $ak_{\parallel}/2\pi$ (0.092°) and 0.011 (0.87°) for OP and PP, respectively, and the corresponding peak shift is 0.0005 (0.04°).

Next we explore the resonant transmission through the 2D nanohole array for sensor applications by introducing an index-calibrated solution through the microfluidic channel to create a controlled gold–fluid interface. We repeat our experiments on angular and wavelength interrogation exciting the $[+1,0]$ type SPP modes and vary the refractive index of the overlayer fluid (varying concentrations of Na_2CrO_4 in H_2O). Since the resolving power and interrogation range are both higher in angular interrogation, we focus our following study on it. Figure 3 shows experimental results on the position of the resonant transmission peak through angu-

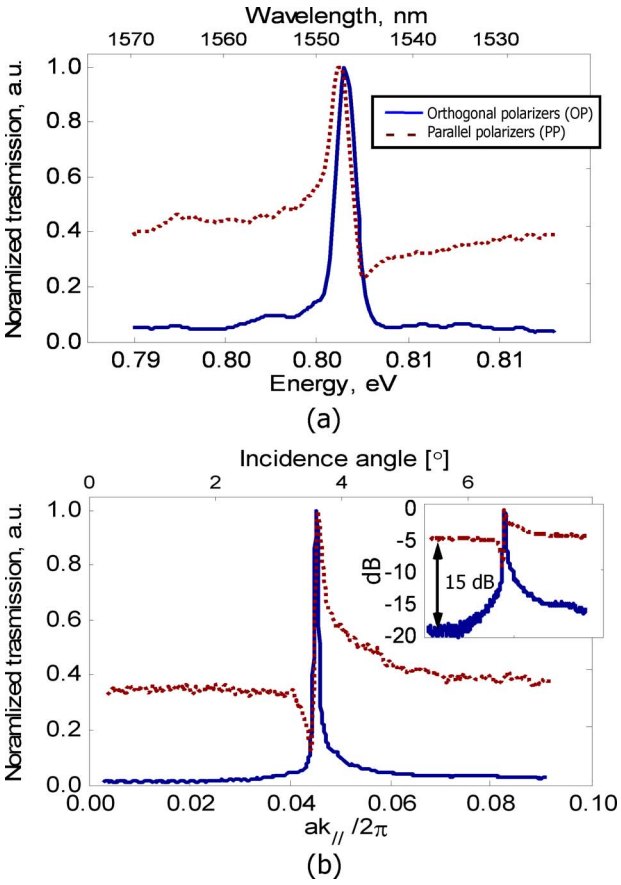

Fig. 2. (Color online) Normalized transmission as a function of (a) energy (wavelength) and (b) parallel wave vector (angle). In each case the dotted curves correspond to the PP and the solid curves correspond to the OP polarization states (as illustrated in Fig. 1 and described in the text). The transmission in each case has been normalized to the maximum to clearly illustrate the respective line-shape functions. Inset in (b) are the same data plotted in a logarithmic scale to show the ~15–20 dB background level reduction for the Lorentzian versus Fano-type resonances.

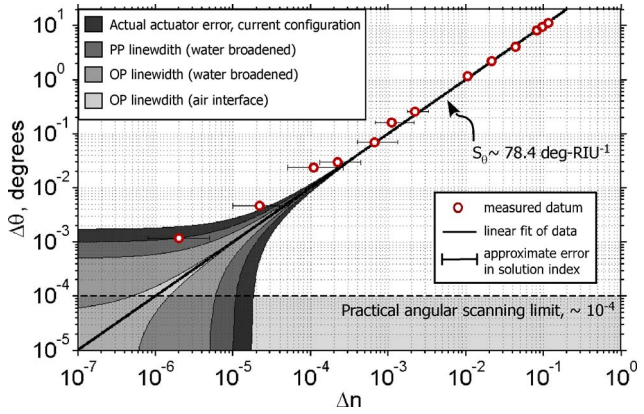

Fig. 3. (Color online) Resonance peak position shift versus refractive index change (i.e., salt concentration in water) in the fluidic overlayer. Black line, linear fit to the data. Shaded regions, approximate peak position (absolute refractive index) errors in the fitting procedure for the OP and PP conditions for both air and water broadened linewidths as well as estimated theoretical resolution limits.

lar interrogation versus the index of refraction of the fluid on the interface. Due to the strong absorption of water in this wavelength range, the linewidths for wavelength and angular interrogation broaden to values of 4.32 meV (8.31 nm) and 0.0064 $ak_{\parallel}/2\pi$ (0.52°), respectively, with OP. At shorter wavelengths the damping due to water is reduced, but the metal losses are larger. Also, at shorter wavelengths there is a greater mode overlap of the resonant field with the reaction of interest as the extent of the mode into the dielectric is reduced. Error bars in the horizontal direction are from uncertainty in the solution index of refraction as well as variations in temperature. Peak positions are determined by both the method of moments (centroid position) and by fitting Lorentzian functions, and the error bounds for these methods in the presence of noise are shown as the various shaded regions. This procedure corresponds to estimated sensing limits of 5×10^{-6} and 1×10^{-5} refractive index units (RIU) for OP and PP, respectively. The darkest region corresponds to the observed error 1.7×10^{-3} (standard deviation) due to lack of full optimization in the feedback controls and therefore limited our direct measurement limit to $\sim1.5\times10^{-5}$. We estimate the limits for a nonabsorbing overlayer (with a gaseous analyte, for example) with OP and an optimized rotation stage (mechanical limits of $\sim10^{-4}$ in angle) to be of the order 1×10^{-6}, which is shown with the lightest shading.

While the peak position is typically determined more precisely, it is useful to introduce the metric $\chi_{\lambda,\theta}\equiv S_{\lambda,\theta}/\Gamma_{\lambda,\theta}$, which is a measure of the resolving power that facilitates comparisons of different sensors and interrogation methods.[18] Here S is the sensitivity (i.e., derivative of the resonance position with respect to the index of refraction), Γ is the FWHM, and the subscripts λ and θ refer to wavelength and angular interrogations, respectively. We experimentally determine $S_\lambda\sim1022\pm8$ nm RIU^{-1} and $S_\theta\sim78.4\pm0.6$ deg RIU^{-1} that yield values of $\chi_\theta\sim850$ RIU^{-1} and $\chi_\lambda\sim410$ RIU^{-1} with an air overlayer, while these values are reduced to $\chi_\theta\sim150$ RIU^{-1} and $\chi_\lambda\sim120$ RIU^{-1} with water broadened transmission. These values compare favorably with values of $\chi_\lambda\sim108(48)$ RIU^{-1} and $\chi_\theta\sim83(48)$ RIU^{-1} for prism (grating) -based sensors, respectively, at 850 nm.

We have demonstrated a high-resolution SPR sensor based on transmission through nanohole arrays. The transmission line-shape function was shown to vary with the input and output polarization states, showing a Fano-type dependence with a pure resonant Lorentzian of minimal width when these two states are orthogonal. In these structures, the SPP propagation length may be reduced (from approximately several tens of micrometers in this case) to increase the spatial resolution and limit the cross talk between channels. This leads to a design trade-off where the spectral or angular resolution (resolving power) may be sacrificed for smaller interrogation volumes depending on the particular application. In addition, one can break the in-plane symmetry and use, for example, elliptical[16] or chiral shaped holes to have polarization dependence even at normal incidence. These results will aid in the development of future nanohole SPR sensors.

We thank the DARPA Optofluidics Center, NSF, and AFOSR for support. K. A. Tetz's e-mail address is ktetz@ucsd.edu.

References

1. J. Homola, S. S. Yee, and G. Gauglitz, Sens. Actuators B **54**, 3 (1999).
2. S. Y. Wu, H. P. Ho, W. C. Law, C. L. Lin, and S. K. Kong, Opt. Lett. **29**, 2378 (2004).
3. I. R. Hopper and J. R. Sambles, Appl. Phys. Lett. **85**, 3017 (2004).
4. J. Dostalek, J. Homola, and M. Miler, Sens. Actuators B **107**, 154 (2005).
5. Y. D. Su, S. J. Chen, and T. L. Yeh, Opt. Lett. **30**, 1488 (2005).
6. T. W. Ebbesen, H. J. Lezec, H. F. Ghaemi, T. Thio, and P. A. Wolff, Nature **391**, 667 (1998).
7. A. G. Brolo, R. Gordon, B. Leathem, and K. L. Kavanagh, Langmuir **20**, 4813 (2004).
8. T. Rindzevicius, Y. Alaverdyan, A. Dahlin, F. Hook, D. S. Sutherland, and M. Kall, Nano Lett. **5**, 2335 (2005).
9. L. Pang, W. Nakagawa, and Y. Fainman, Appl. Opt. **42**, 5450 (2003).
10. K. A. Tetz, R. Rokitski, M. Nezhad, and Y. Fainman, Appl. Phys. Lett. **86**, 111110 (2005).
11. V. Lomakin and E. Michielssen, Phys. Rev. B **71**, 235117 (2005).
12. C. Genet, M. P. van Exter, and J. P. Woerdman, Opt. Commun. **225**, 331 (2003).
13. M. Sarrazin, J. P. Vigneron, and J. M. Vigoureux, Phys. Rev. B **67**, 085415 (2003).
14. R. Muller, V. Malyarchuk, and C. Lienau, Phys. Rev. B **68**, 205415 (2003).
15. W. L. Barnes, W. A. Murray, J. Dintinger, E. Devaux, and T. W. Ebbesen, Phys. Rev. Lett. **92**, 107401 (2004).
16. J. Elliott, I. I. Smolyaninov, N. I. Zheludev, and A. V. Zayats, Opt. Lett. **29**, 1414 (2004).
17. S. J. Elston, G. P. Bryan-Brown, and J. R. Sambles, Phys. Rev. B **44**, 6393 (1991).
18. J. Homola, I. Koudela, and S. S. Yee, Sens. Actuators B **54**, 16 (1999).